2012

KFe2Se2 is the Parent Compound of K-Doped Iron Selenide Superconductors

Weijie Li
Tsinghua University, weijie@uow.edu.au

Hao Ding
Tsinghua University

Zhi Li
Chinese Academy of Sciences, zhili@uow.edu.au

Peng Deng
Tsinghua University

Kai Chang
Tsinghua University

See next page for additional authors

Publication Details

Li, W., Ding, H., Li, Z., Deng, P., Chang, K., He, K., Ji, S., Wang, L., Ma, X., Hu, J., Chen, X. & Xue, Q. (2012). KFe2Se2 is the Parent Compound of K-Doped Iron Selenide Superconductors. Physical Review Letters, 109 057003-1-057003-5.

KFe2Se2 is the Parent Compound of K-Doped Iron Selenide Superconductors

Abstract
We elucidate the existing controversies in the newly discovered K-doped iron selenide (KxFe2ySe2z) superconductors. The stoichiometric KFe2Se2 with ffiffiffi 2 p ffiffiffi 2 p charge ordering was identified as the parent compound of KxFe2ySe2z superconductor using scanning tunneling microscopy and spectroscopy. The superconductivity is induced in KFe2Se2 by either Se vacancies or interacting with the antiferromagnetic K2Fe4Se5 compound. In total, four phases were found to exist in KxFe2ySe2z: parent compound KFe2Se2, superconducting KFe2Se2 with ffiffiffi 2 p ffiffiffi 5 p charge ordering, superconducting KFe2Se2z with Se vacancies, and insulating K2Fe4Se5 with ffiffiffi 5 p ffiffiffi 5 p Fe vacancy order. The phase separation takes place at the mesoscopic scale under standard molecular beam epitaxy conditions. D

Keywords
parent, k-doped, kfe2se2, iron, selenide, superconductors, compound

Disciplines
Engineering | Physical Sciences and Mathematics

Publication Details
Li, W., Ding, H., Li, Z., Deng, P., Chang, K., He, K., Ji, S., Wang, L., Ma, X., Hu, J., Chen, X. & Xue, Q. (2012). KFe2Se2 is the Parent Compound of K-Doped Iron Selenide Superconductors. Physical Review Letters, 109 057003-1-057003-5.

Authors
Weijie Li, Hao Ding, Zhi Li, Peng Deng, Kai Chang, Ke He, Shuaihua Ji, Lili Wang, Xu-Cun Ma, Jiang-Ping Hu, Xi Chen, and Qi-Kun Xue

KFe_2Se_2 is the Parent Compound of K-Doped Iron Selenide Superconductors

Wei Li,[1] Hao Ding,[1] Zhi Li,[2] Peng Deng,[1] Kai Chang,[1] Ke He,[2] Shuaihua Ji,[1] Lili Wang,[2] Xucun Ma,[2] Jiang-Ping Hu,[3] Xi Chen,[1,*] and Qi-Kun Xue[1,†]

[1]*State Key Laboratory of Low-Dimensional Quantum Physics, Department of Physics, Tsinghua University, Beijing 100084, China*
[2]*Institute of Physics, Chinese Academy of Sciences, Beijing 100190, China*
[3]*Department of Physics, Purdue University, West Lafayette, Indiana 47907, USA*

(Received 7 April 2012; published 31 July 2012)

We elucidate the existing controversies in the newly discovered K-doped iron selenide ($K_xFe_{2-y}Se_{2-z}$) superconductors. The stoichiometric KFe_2Se_2 with $\sqrt{2} \times \sqrt{2}$ charge ordering was identified as the parent compound of $K_xFe_{2-y}Se_{2-z}$ superconductor using scanning tunneling microscopy and spectroscopy. The superconductivity is induced in KFe_2Se_2 by either Se vacancies or interacting with the antiferromagnetic $K_2Fe_4Se_5$ compound. In total, four phases were found to exist in $K_xFe_{2-y}Se_{2-z}$: parent compound KFe_2Se_2, superconducting KFe_2Se_2 with $\sqrt{2} \times \sqrt{5}$ charge ordering, superconducting KFe_2Se_{2-z} with Se vacancies, and insulating $K_2Fe_4Se_5$ with $\sqrt{5} \times \sqrt{5}$ Fe vacancy order. The phase separation takes place at the mesoscopic scale under standard molecular beam epitaxy conditions.

DOI: 10.1103/PhysRevLett.109.057003 PACS numbers: 74.70.Xa, 64.75.Jk, 73.20.−r, 74.55.+v

Similar to cuprate high temperature superconductors, superconductivity in pnictides and chalcogenides is induced by suppressing the magnetic order in their iron-based parent compounds [1–4]. Therefore, understanding the parent compounds is crucial for elucidating the superconducting pairing mechanism. For most of the Fe-based superconductors, it is straightforward to identify their parent compounds. However, the newly discovered K-doped iron selenide superconductor [$K_xFe_{2-y}Se_{2-z}$, lattice structure of KFe_2Se_2 is shown in Fig. 1(a)] [5–7] has been shown to be unique [8–19], and the parent compound of this hotly debated material remains elusive. The central issue being debated is the role of the $K_2Fe_4Se_5$ compound with $\sqrt{5} \times \sqrt{5}$ Fe vacancy order. $K_2Fe_4Se_5$ is one of the coexisting phases in $K_xFe_{2-y}Se_{2-z}$ [14–18] and has an antiferromagnetic order with a Néel temperature up to 560 K [9,10]. Several experiments [7–13] have shown that $K_2Fe_4Se_5$ has a close connection with the superconductivity in $K_xFe_{2-y}Se_{2-z}$ and suggested that $K_2Fe_4Se_5$ is the parent compound. However, the scanning tunneling microscopy (STM) data, on the other hand, indicate that the superconducting phase in $K_xFe_{2-y}Se_{2-z}$ is the stoichiometric KFe_2Se_2 compound [18].

Although our previous study identified KFe_2Se_2 as a superconductor [18], we have not yet answered the question of why the insulating $K_2Fe_4Se_5$ is closely related to the superconductivity in K-doped iron selenide. In the (110) film on graphitized SiC substrate [18], KFe_2Se_2 and $K_2Fe_4Se_5$ phases coexist side by side and the phase separation is roughly along the c axis. To understand the role of $K_2Fe_4Se_5$, one needs a control experiment where the phase separation is in different configurations. In the present work, we grow high-quality $K_xFe_{2-y}Se_{2-z}$ thin films on $SrTiO_3(001)$ substrate by using molecular beam epitaxy (MBE). The orientation of the film on $SrTiO_3$ is the natural cleavage plane (001) instead of (110) on graphitized SiC. The subsequent STM measurement demonstrates two different phase separation configurations: either along the c-axis or in the a-b plane. The metallic KFe_2Se_2 with $\sqrt{2} \times \sqrt{2}$ charge ordering is identified as the parent compound. Superconductivity is induced in this parent compound only when the phase separation is along the c axis. These findings explain the apparent coexistence of magnetism and superconductivity in $K_xFe_{2-y}Se_{2-z}$: Although $K_2Fe_4Se_5$ with $\sqrt{5} \times \sqrt{5}$ Fe vacancy order is not superconducting by itself, it can give rise to superconductivity in KFe_2Se_2.

Our experiments were conducted with a Unisoku UHV 3He STM system that reaches a base temperature of 0.4 K by means of a single-shot 3He cryostat. The bias voltage is applied to the sample. High-purity Fe (99.995%), Se (99.9999%), and K were evaporated from two standard Knudsen cells and one alkali-metal dispenser (SAES Getters), respectively. The substrate was held at 400 °C during growth. The MBE growth of the film follows the layer-by-layer mode. To remove the extra K and Se adatoms and obtain the superconducting phase, the sample was subsequently annealed at 400 °C for one hour. The STM experiments were performed in the same ultrahigh vacuum system. Figure 1(b) shows the typical topography of a film after annealing. The step height is 0.7 nm and in good agreement with the lattice parameter of KFe_2Se_2. The K atoms on the topmost layer are highly mobile and most of them can be easily desorbed during annealing; thus the film is Se-terminated. We attribute the protrusions on the surface in Fig. 1(b) to the residual K clusters. The STM image with atomic resolution in Fig. 1(c) shows a 3.9 Å × 3.9 Å square lattice consistent with the X-ray data for (001) plane of KFe_2Se_2 [5]. Therefore, the surface is that of a stoichiometric KFe_2Se_2 single-crystalline film and no surface reconstruction is observed.

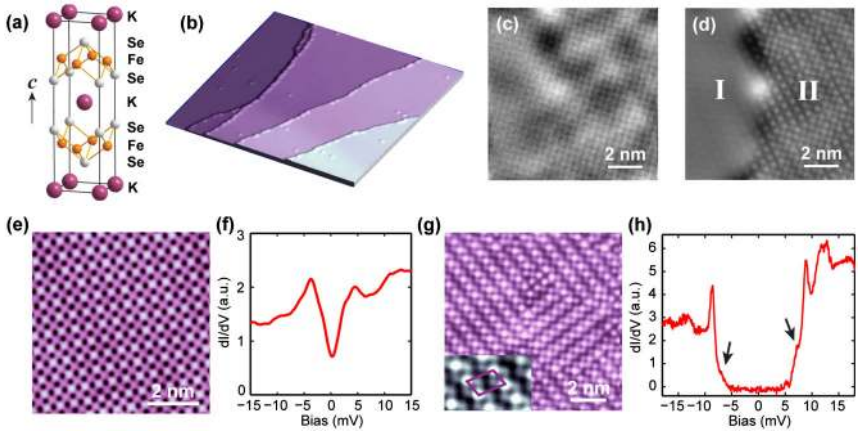

FIG. 1 (color online). STM characterization of $K_xFe_{2-y}Se_2$ films grown by MBE. (a) The crystal structure of KFe_2Se_2. (b) Topographic image (3.9 V, 0.02 nA, 90×90 nm) of a $K_xFe_{2-y}Se_2$ film. (c) and (d) Atomic-resolution STM topography (10×10 nm) of KFe_2Se_2. The two images belong to the same area, but with different bias voltages: -90 mV for (c) and 50 mV for (d). The tunneling current is 0.02 nA for both. Panel (c) shows the uniform 1×1-Se square lattice. Inhomogeneity in electronic structure is revealed in (d) with two distinct regions labeled by I and II. The area ratio between I and II is about 1:5. (e) The $\sqrt{2} \times \sqrt{2}$ charge ordering in region I. The imaging condition: 40 mV, 0.02 nA. (f) dI/dV spectrum (set point, 25 mV, 0.1 nA) of region I, which reveals that region I is nonsuperconducting. (g) The $\sqrt{2} \times \sqrt{5}$ charge ordering (see also inset) in region II. Imaging condition: 30 mV, 0.02 nA. (h) dI/dV spectrum (0.4 K; set point, 20 mV, 0.1 nA) showing that there is a superconducting gap opened in region II. Arrows mark the smaller gap.

Although the lattice structure is uniform throughout the film surface, inhomogeneity in the electronic structure is clearly revealed by STM. Figure 1(c) and 1(d) are the STM images of the same area, but with different bias voltages. In Fig. 1(d), the film is separated into two regions labeled I and II, while the 1×1-Se square lattice is uninterrupted when crossing the boundary of the two regions [Fig. 1(c)]. At a bias voltage within ± 100 mV, region I exhibits a $\sqrt{2} \times \sqrt{2}$ superstructure [14,19] [Fig. 1(e)] with respect to the original Se lattice. The $\sqrt{2} \times \sqrt{2}$ charge ordering has its origin in the block antiferromagnetic state of the underlying Fe layer [20]. In the ground state of KFe_2Se_2, each four Fe atoms group together to form a checkerboard pattern with antiferromagnetic order, leading to a charge density modulation on Se sites. This checkerboard phase driven by magnetic exchange coupling breaks the original symmetry of the tetragonal lattice but still retains a fourfold symmetry.

Scanning tunneling spectroscopy (STS) probes the local density of states of electrons. The STS of region I shows a 10 mV dip near the Fermi level [Fig. 1(f)]. The same feature was also observed on the cleaved $K_xFe_{2-y}Se_2$ single crystal [19]. The dip may stem from the $\sqrt{2} \times \sqrt{2}$ charge ordering but does not imply superconductivity because the bottom of the dip still has finite density of states and the spectrum is essentially independent of temperature from 0.4 to 4.2 K. Therefore, region I is a nonsuperconductive metal.

We observe a different charge ordering in region II [Fig. 1(g)]. The fret-like pattern breaks the fourfold symmetry and is visible within a bias voltage of ± 60 mV. The pattern is an electronic feature instead of surface reconstruction because of the strong bias-dependency (see also Supplemental Material [21]). The basic building block of the pattern is a $\sqrt{2} \times \sqrt{5}$ charge density modulation [see the parallelogram in the inset of Fig. 1(g)]. The region is divided into domains depending on the orientations of the stripes.

The STS of region II [Fig. 1(h)] exhibits a full energy gap centered at Fermi level and two pronounced coherence peaks, indicating that region II is superconducting with a nearly isotropic gap. The superconducting gap $\Delta = 8.8$ meV is estimated by half of the energy between the two coherence peaks and in close agreement with that obtained by angle-resolved photoemission spectroscopy [22–27]. Angle-resolved photoemission spectroscopy measurement [22,26,27] also found a smaller gap on the pockets at Z point. In STS, the smaller gap is indicated by the shoulders at ± 7.2 meV [marked by arrows in Fig. 1(h)]. The feature at 13 mV, which can be attributed to a bosonic excitation mode, is insensitive to magnetic field and spatially dependent (see Supplemental Material [21]).

Although it is not feasible to do transport measurement on the $K_xFe_{2-y}Se_{2-z}$ film at present, the occurrence of superconductivity is further supported by the response of STS to external magnetic field or magnetic defects. Similar to $KFe_2Se_2(110)$ film [18], no magnetic vortex is observed in the superconducting state of region II. Nevertheless, the effect of magnetic field is still manifested itself by reducing the coherence peaks in STS (see supporting material [21]). Stronger suppression of the coherence peaks can be achieved by magnetic defects [28–30], which locally break the time-reversal symmetry (Fig. 2). Both Fe and Se vacancies carry magnetic moment and induce bound

quasiparticle states in the superconducting gap [Fig. 2(b) and 2(d)]. A distinct feature of such bound states in a superconductor is that the energies of the electronlike and holelike states are symmetric with respect to zero bias whereas their amplitudes are usually different as a result of on-site Coulomb interaction [31].

KFe_2Se_2 in region I and II has the same crystal structure but exhibits very different electronic properties. We attribute the difference to the existence of antiferromagnetic $K_2Fe_4Se_5$ insulating layer below the KFe_2Se_2 film in region II [see the schematic in Fig. 3(a)]. Although $K_2Fe_4Se_5$ layer is a few nanometers below the surface, its $\sqrt{5} \times \sqrt{5}$ Fe vacancy order is still visible in STM image at 70 mV [Fig. 3(b)] due to the three-dimensional tunneling effect [32]. The dashed circles in Fig. 3(b) highlight some of the atoms forming the $\sqrt{5} \times \sqrt{5}$ pattern. The projection of interface structure to the topmost surface has been observed in other systems [33–35] and usually happens in a sample with high quality. The existence of $K_2Fe_4Se_5$ layer below KFe_2Se_2 is further supported by the well-defined moiré pattern marked by arrows in the STM image in Fig. 3(b). The period of the pattern is $3\sqrt{5}a_{Se}$, where a_{Se} is the Se-Se distance. The Moiré pattern is in excellent agreement with a simple simulation (see Supplemental Material [21]), where two lattices with $\sqrt{2} \times \sqrt{5}$ and $\sqrt{5} \times \sqrt{5}$ superstructures are superimposed on each other.

STM imaging of the films indicates that the growth condition in the present work always produces a film with KFe_2Se_2 phase on the top and no $K_2Fe_4Se_5$ phase is exposed. The possible reason is that Se is highly volatile and the Se-rich phase in the top few layers is kinetically unstable under the growth temperature. In further investigation, fine-tuning of growth conditions may alter the surface stoichiometry and lead to a film with $K_2Fe_4Se_5$ phase on the top surface.

Phase separation between superconducting KFe_2Se_2 and insulating $K_2Fe_4Se_5$ along the c axis has previously been demonstrated [14,18,36]. However, not all KFe_2Se_2 is superconducting. Here we have shown that the nonsuperconductive phase of KFe_2Se_2 has a $\sqrt{2} \times \sqrt{2}$ charge ordering, which becomes superconducting only when it interfaces with $K_2Fe_4Se_5$ and develops a $\sqrt{2} \times \sqrt{5}$ charge ordering. For this reason, it is appropriate to identify KFe_2Se_2 with $\sqrt{2} \times \sqrt{2}$ charge ordering as the parent compound. Similar to the $\sqrt{2} \times \sqrt{2}$ charge ordering, the $\sqrt{2} \times \sqrt{5}$ pattern may also be the result of a specific type of magnetic ordering in the Fe layer of KFe_2Se_2 (one possibility is shown in the Supplemental Material [21]).

There are various ways, such as strain, magnetic coupling, or charge transfer, that the $K_2Fe_4Se_5$ layer can regulate the electronic properties of KFe_2Se_2. Strain effect can be simply excluded because the lattice constants of $K_2Fe_4Se_5$ are very close to those of KFe_2Se_2. An analogy to cuprate high-temperature superconductors suggests that the $K_2Fe_4Se_5$ layer may play the role as charge reservoir

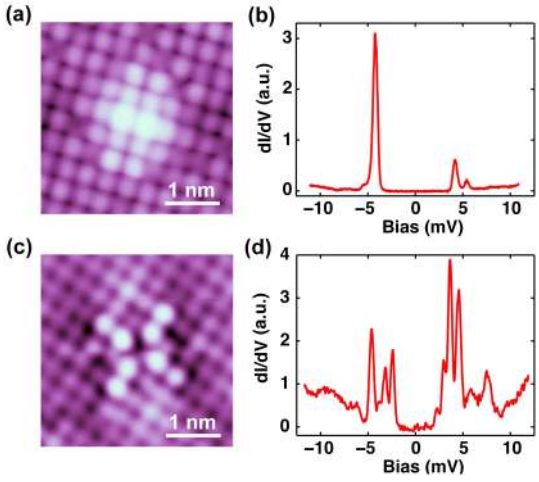

FIG. 2 (color online). Vacancy-induced bound states in superconducting gap. (a) and (b) STM topography (40 mV, 0.02 nA) and dI/dV spectrum (0.4 K; set point, 25 mV, 0.1 nA) of a single Fe vacancy. The defect is attributed to Fe vacancy by examining the symmetry of the STM image. (c) and (d) STM topography ($-$ 95 mV, 0.02 nA) and dI/dV spectrum (0.4 K; set point, 25 mV, 0.1 nA) of a single Se vacancy. The magnetic moment of a Se vacancy comes from the four adjacent Fe atoms. More bound states are induced by the Se vacancy because of the lower spatial symmetry.

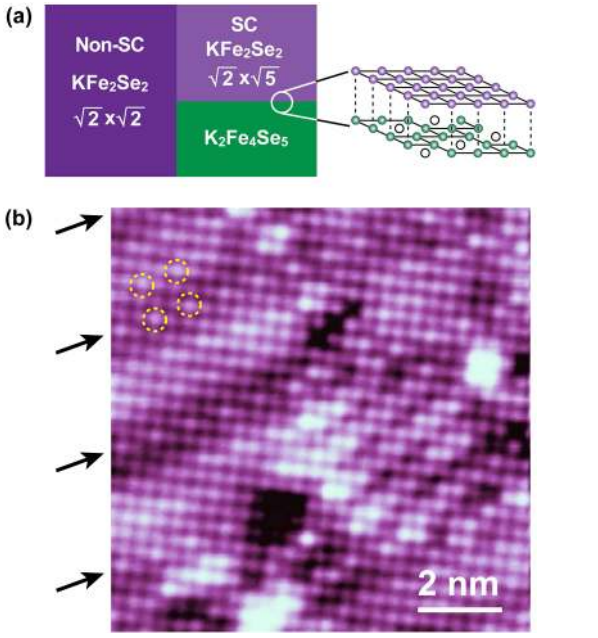

FIG. 3 (color online). The origin of superconductivity in KFe_2Se_2. (a) Schematic showing the relationship between insulating $K_2Fe_4Se_5$ and superconducting KFe_2Se_2. Across the interface between KFe_2Se_2 and $K_2Fe_4Se_5$, the lattice structure is the same except for a $\sqrt{5} \times \sqrt{5}$ Fe vacancy order in $K_2Fe_4Se_5$. (b) $\sqrt{5} \times \sqrt{5}$ superstructure in region II. The image belongs to the same area as Fig. 1(g), but with a different bias voltage (70 mV). The Moiré pattern is marked by arrows.

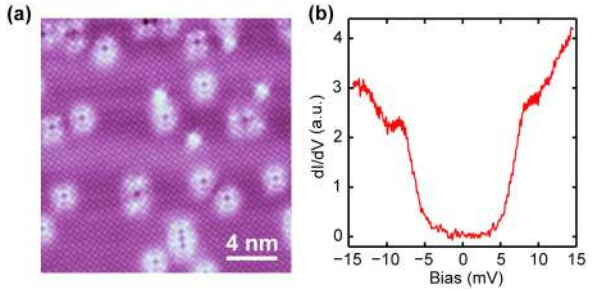

FIG. 4 (color online). Superconductivity in KFe_2Se_{2-z}. (a) STM topography (75 mV, 0.02 nA) of an area with Se vacancies. (b) Superconducting gap (0.4 K; set point, 25 mV, 0.1 nA) at a location away from Se vacancies.

and transfer carriers into KFe_2Se_2 to induce superconductivity. To keep the balance of chemical valence, the KFe_2Se_2 phase tends to lose electrons and becomes hole-doped in the superconducting state. Another possibility is that the antiferromagnetic $K_2Fe_4Se_5$ may change the magnetic structure of KFe_2Se_2 through their exchange coupling across the interface, and KFe_2Se_2 becomes superconducting after the original C_4 symmetry is broken by the magnetic interaction. In all scenarios, the interface between KFe_2Se_2 and $K_2Fe_4Se_5$ is a key factor. The interface in the present (001) film is more regular than that in the (110) film grown on graphitized SiC [18]. In the (110) film, the boundary between KFe_2Se_2 and $K_2Fe_4Se_5$ is not flat but always wanders across different *a*-*b* planes. The difference may help to explain the larger superconducting gap observed in this work.

Interfacing with $K_2Fe_4Se_5$ is not the only way to induce superconductivity in the parent compound KFe_2Se_2. Superconductivity can also occur in a film with a certain amount of Se-vacancies (with a density of about one in 10 nm^2). The quatrefoil-like defects [Fig. 4(a)] appear if the substrate temperature is raised to 430 °C during growth. The defects are attributed to Se vacancies by examining their registration with respect to the lattice. The film shows the same $\sqrt{2} \times \sqrt{2}$ superstructure as the parent compound. No sign of $\sqrt{5} \times \sqrt{5}$ Fe vacancy order has been observed. STS [Fig. 4(b)] at a location away from Se vacancies exhibits a very similar superconducting gap to that on KFe_2Se_2 with $\sqrt{2} \times \sqrt{5}$ charge ordering [Fig. 1(h)]. The coherence peaks are weaker than those in Fig. 1(h) because of the existence of defects. The Se vacancies carry magnetic moment, giving rise to bound states (see Supplemental Material [21]) similar to those in Fig. 2(d). The vacancies break the magnetic ordering in KFe_2Se_2 and induce superconductivity in the parent compound. The disorder-induced superconductivity exists in other iron-based superconductors as well, for example, $Ba(Fe_{1-x}Ru_x)_2As_2$ [37] and $BaFe_2(As_{1-x}P_x)_2$ [38] where Fe and As are iso-valently substituted by Ru and P, respectively. Uncovering this second path leading to superconductivity indicates that it is possible to prepare a superconducting KFe_2Se_{2-z} sample without $\sqrt{5} \times \sqrt{5}$ Fe vacancy order.

By demonstrating two different ways to induce superconductivity in the parent compound KFe_2Se_2, we have elucidated the existing controversies in K-doped iron selenide superconductors. The apparent coexistence of superconductivity and antiferromagnetism with large magnetic moment is, as a matter of fact, a "symbiotic" relationship taking place at the mesoscopic scale. These findings may open a new avenue for manipulating the superconducting properties of materials.

We thank X. J. Chen and J. X. Zhu for valuable discussions. The work is supported by NSFC and the National Basic Research Program of China. The STM topographic images were processed using WSxM (www.nanotec.es).

*xc@mail.tsinghua.edu.cn
†qkxue@mail.tsinghua.edu.cn

[1] J. Paglione and R. L. Greene, Nature Phys. **6**, 645 (2010).
[2] D. C. Johnston, Adv. Phys. **59**, 803 (2010).
[3] P. J. Hirschfeld, M. M. Korshunov, and I. I. Mazin, Rep. Prog. Phys. **74**, 124508 (2011).
[4] G. R. Stewart, Rev. Mod. Phys. **83**, 1589 (2011).
[5] J. G. Guo, S. F. Jin, G. Wang, S. C. Wang, K. X. Zhu, T. T. Zhou, M. He, and X. L. Chen, Phys. Rev. B **82**, 180520(R) (2010).
[6] A. F. Wang *et al.*, Phys. Rev. B **83**, 060512(R) (2011).
[7] M.-H. Fang, H.-D. Wang, C.-H. Dong, Z.-J. Li, C.-M. Feng, J. Chen, and H. Q. Yuan, Europhys. Lett. **94**, 27009 (2011).
[8] Z. Shermadini *et al.*, Phys. Rev. Lett. **106**, 117602 (2011).
[9] W. Bao, Q.-Z. Huang, G.-F. Chen, M. A. Green, D.-M. Wang, J.-B. He, and Y.-M. Qiu, Chin. Phys. Lett. **28**, 086104 (2011).
[10] V. Yu. Pomjakushin, D. V. Sheptyakov, E. V. Pomjakushina, A. Krzton-Maziopa, K. Conder, D. Chernyshov, V. Svitlyk, and Z. Shermadini, Phys. Rev. B **83**, 144410 (2011).
[11] Y. J. Yan *et al.*, Sci. Rep. **2**, 212 (2012).
[12] P. Zavalij *et al.*, Phys. Rev. B **83**, 132509 (2011).
[13] W. Bao *et al.*, arXiv:1102.3674.
[14] Z. Wang, Y. J. Song, H. L. Shi, Z. W. Wang, Z. Chen, H. F. Tian, G. F. Chen, J. G. Guo, H. X. Yang, and J. Q. Li, Phys. Rev. B **83**, 140505(R) (2011).
[15] B. Shen, B. Zeng, G. F. Chen, J. B. He, D. M. Wang, H. Yang, and H. H. Wen, Europhys. Lett. **96**, 37010 (2011).
[16] A. Ricci *et al.*, Phys. Rev. B **84**, 060511(R) (2011).
[17] F. Chen *et al.*, Phys. Rev. X **1**, 021020 (2011).
[18] W. Li *et al.*, Nature Phys. **8**, 126 (2012).
[19] P. Cai, C. Ye, W. Ruan, X. D. Zhou, A. F. Wang, M. Zhang, X. H. Chen, and Y. Y. Wang, Phys. Rev. B **85**, 094512 (2012).
[20] W. Li, S. Dong, C. Fang, and J. Hu, Phys. Rev. B **85**, 100407(R) (2012).
[21] See Supplemental Material at http://link.aps.org/supplemental/10.1103/PhysRevLett.109.057003 for additional materials about the experimental results.

[22] Y. Zhang *et al.*, Nature Mater. **10**, 273 (2011).
[23] T. Qian *et al.*, Phys. Rev. Lett. **106**, 187001 (2011).
[24] L. Zhao *et al.*, Phys. Rev. B **83**, 140508(R) (2011).
[25] X.-P. Wang, T. Qian, P. Richard, P. Zhang, J. Dong, H.-D. Wang, C.-H. Dong, M.-H. Fang, and H. Ding, Europhys. Lett. **93**, 57001 (2011).
[26] M. Xu *et al.*, Phys. Rev. B **85**, 220504(R) (2012).
[27] X.-P. Wang *et al.*, arXiv:1205.0996.
[28] A. Yazdani, B. A. Jones, C. P. Lutz, M. F. Crommie, and D. M. Eigler, Science **275**, 1767 (1997).
[29] A. V. Balatsky, I. Vekhter, and J.-X. Zhu, Rev. Mod. Phys. **78**, 373 (2006).
[30] S. H. Ji, T. Zhang, Y.-S. Fu, X. Chen, X.-C. Ma, J. Li, W.-H. Duan, J.-F. Jia, and Q.-K. Xue, Phys. Rev. Lett. **100**, 226801 (2008).
[31] M. I. Salkola, A. V. Balatsky, and J. R. Schrieffer, Phys. Rev. B **55**, 12648 (1997).
[32] K. Kobayashi, Phys. Rev. B **53**, 11091 (1996).
[33] M. Yakes and M. C. Tringides, J. Phys. Chem. A **115**, 7096 (2011).
[34] Y.-S. Fu, S.-H. Ji, T. Zhang, X. Chen, J.-F. Jia, Q.-K. Xue, and X.-C. Ma, Chin. Phys. Lett. **27**, 066804 (2010).
[35] F. Cheng *et al.*, arXiv:1102.1056.
[36] A. Charnukha *et al.*, Phys. Rev. Lett. **109**, 017003 (2012).
[37] R. S. Dhaka *et al.*, Phys. Rev. Lett. **107**, 267002 (2011).
[38] S. Jiang, H. Xing, G. F. Xuan, C. Wang, Z. Ren, C. M. Feng, J. H. Dai, Z. A. Xu, and G. H. Cao, J. Phys. Condens. Matter **21**, 382203 (2009).